Article

Simulations of Structures in Packed Columns and Validation by X-ray Tomography

R. Caulkin, X. Jia, C. Xu, M. Fairweather, R. A. Williams, H. Stitt, M. Nijemeisland, S. Aferka, M. Crine, A. Le#onard, D. Toye, and P. Marchot

Ind. Eng. Chem. Res., **2009**, 48 (1), 202-213 • DOI: 10.1021/ie800033a • Publication Date (Web): 14 August 2008

Simulations of Structures in Packed Columns and Validation by X-ray Tomography

R. Caulkin,[†] X. Jia,*[,†] C. Xu,[‡] M. Fairweather, R. A. Williams,[†] H. Stitt,[§] M. Nijemeisland,[§] S. Aferka,[||] M. Crine,[||] A. Léonard,[||] D. Toye,[||] and P. Marchot[||]

Institute of Particle Science and Engineering, School of Process, Environmental and Materials Engineering, University of Leeds, Leeds LS2 9JT, United Kingdom, Structure Vision Ltd., Leeds Innovation Centre, 103 Clarendon Road, Leeds LS2 9DF, United Kingdom, Johnson Matthey Catalysts, P.O. Box No 1, Billingham, Stockton-on-Tees TS23 1LB, United Kingdom, and Chemical Engineering Laboratory, Institut de Chimie, B6c, Université de Liège, Sart Tilman, B4000 Liège, Belgium

Packing simulations of generic, nonspherical pellets were performed and compared with experimental data sets obtained using X-ray computerized tomography (CT). Two modified versions of what was previously a purely geometrical, digitally based packing algorithm were implemented. Both are aimed at incorporating the effects of particle interaction forces, one utilizing the distinct element method (DigiDEM) and the other an intermediate solution (collision-guided packing or DigiCGP). This article summarizes the models and the simulations performed using these two modified versions of DigiPac and, for model validation purposes, compares the predicted results with the corresponding X-ray tomographic scans of packed columns, in terms of bulk density, local packing density profiles, and pellet orientation distributions. For packed beds of relatively large and identical pellets, the simulation results indicate that particle−particle and particle−wall interactions cannot be ignored if realistic packing structures are to be obtained by simulation and even a simplistic treatment of these interactions can produce significantly more realistic packing structure than none at all.

1. Introduction

Packed columns, because of their large internal specific surface areas and hence high mass- and heat-transfer rates, are used in a multitude of industrial processes.[1] To design and control these systems effectively, a variety of problems must be addressed. Among those that merit investigation, this study considers the ability of a digitally based particle packing algorithm, called DigiPac, to predict bulk and local packing densities and pellet orientation in a variety of nonspherical beds. The final packing structure of such beds is of great interest because it influences subsequent properties such as fluid dynamics, heat transfer, mixing, and contacting surfaces. Precision in the evaluation of properties such as packing density and pellet orientation distribution have the potential to impact on future chemical reactor design parameters. For example, advances in prediction methods could lead to improvements, refinements, and even quantification of the effects of different variables such as loading method, container shape/size, and interfacial area on bed structure.

Traditionally, the main parameter used in characterizing the packing structure of any particulate assembly is the mean voidage, defined as the ratio of the void volume to the total volume of the packed bed. Local voidage is the ratio of the void volume to the volume of the packed bed in a localized area of the packing, usually categorized into three types: axial, radial, and angular. The mean and local voidages of packed beds have been investigated extensively using various experimental and analytical methods.[2−4] However, despite the volume of work that has been undertaken on packed columns[5] in attempts to quantify their structural properties, such studies generally result in empirical correlations that are pellet-geometry-dependent and thus of limited use. Therefore, as yet, there is still no definitive method with which to predict the porosity of a bed comprosed of various regular- or irregular-shaped particles. This article presents the results of the DigiPac approach to predicting the structure of such beds. The key to this method is that a digital representation of the particles and the packing space is used, avoiding many of the difficulties associated with traditional vector-based approaches, thereby providing a relatively straightforward and efficient means to pack particles of any shape into containers of arbitrary geometries. The ethos of the original DigiPac algorithm,[6] which is also carried across to the modified versions, is to map the particles, the packing space (container), and the particle movement onto a regular lattice grid. Therefore, the shape of a particle, no matter how complex, is simply a coherent collection of pixels (2D) or voxels (3D) that are allowed to move randomly, one grid space at a time, within the specified boundaries of a container. This greatly simplifies the representation and manipulation of complex-shaped objects in a computer simulation environment.

For rigorously tapped packed columns of relatively large nonspherical objects, preliminary tests have shown that the original DigiPac algorithm often fails to provide a quantitatively close match with experimental observations. For example, in a packing of short cylinders, if the particles are allowed to rotate freely and to vibrate, they tend to end up stacking on top of one another to form an ordered packing structure. Although such an ordered structure can occur in reality for packed beds subjected to long and rigorous vibrations,[7] it is not observed in packed columns of interest to this investigation. Alternatively, if particles are not permitted to rotate (tumble), the predicted bulk density follows the measured trend only qualitatively as pellet geometry changes, and pellet orientations are unrealistic because, without rotation, they remain unchanged from the initial random input. In cases such as this, the completely random

* To whom correspondence should be addressed. E-mail: x.jia@leeds.ac.uk. Tel./Fax: (01943) 872786.
[†] University of Leeds.
[‡] Structure Vision Ltd.
[§] Johnson Matthey Catalysts.
[||] Université de Liège.

10.1021/ie800033a CCC: $40.75
Published on Web 08/14/2008

motion used in the original DigiPac algorithm needs to be replaced with a more realistic motion, determined or at least guided by particle−particle and particle−wall interactions. To this end, two new versions of DigiPac have been developed: DigiDEM and DigiCGP. DigiDEM is a digital implementation of the distinct element method, and DigiCGP is a collision-guided digital packing model. The main highlight of how the modified simulation models provide improvement over the earlier DigiPac method is that the new models include particle interaction forces and so are able to predict, in a more realistic manner, the packing structures of nonspherical particles undergoing rotation, vibration, and tapping. An overview of the models is given in section 2.

Recent advances in tomographic measurement techniques, in particular, nonmedical X-ray computed tomography (CT) scanners designed for material characterization, allow for detailed noninvasive measurements of internal structures. X-ray tomography, as employed in this study to obtain experimental data for model validation, allows detailed microstructural information of packed beds to be obtained faster and more accurately than traditional experimental methods.[5] The collection of X-ray tomographic data presented is, in its own right, a useful contribution to the current knowledge base of packed columns. Although many case-study investigations of X-ray microtomography (XMT) beds have been reported in the literature, this is the first extensive and systematic study, known to us, of nonspherical packed columns using X-ray tomography and provides clear evidence for catalyst manufacturers and users to check their beliefs and empirical relations with regard to microstructures in packed beds.

Despite the volume of published work that has utilized XMT for packed-bed analysis, many studies have resulted in single-case analyses to characterize bed structure or to validate a proposed packing model. Notably, an early investigation in which XMT was utilized to analyze packing structure used a single test sample of about 2000 spheres.[8] In later work, XMT was used to assess polydisperse assemblies, with a sample of approximately 15000 spheres.[9] Additionally, the disordered geometrical structure of an even larger test sample, consisting of 150000 monosized spheres, was investigated by means of X-ray CT.[10] The beads used were around 1 mm in diameter, and a range of packing densities were reported (between 0.58 and 0.64). This work also searched for signatures of disorder in packed beds of spheres. Work focusing on nonspherical particles is scarcer, and as a result, these packing structures are not as well understood or as well characterized as those of spheres. An experimental investigation into the packing of a single type of equilateral cylinder ($L = D = 1.8$ mm) in a tubular container ($D = 23$ mm) using XMT imaging has been reported.[11] The analysis performed included bulk and local porosities, radial distribution functions, and parameters describing local and global orientations of each pellet in an attempt to characterize the packing and void structure of the bed. Using these data sets, changes in the packing structure as a function of increasing packing density were analyzed.

2. Model Description

The original DigiPac model was essentially a Monte Carlo geometrical packing algorithm that did not explicitly consider any physical interaction forces. Implicitly, the effect of gravity was included by way of a rebounding probability. A value of 0 allowed no vertical vibration, and a value of 1 gave equal opportunity for the particles to move up or down and, thus, no chance to settle and form a dense packing; the particles remained suspended, and when more particles were added from the top, thus creating a concentration gradient, they diffused downward. For particles already packed in the sediment, a nonzero rebounding probability provided a nonphysical way to simulate the effects of vibration whereby particles, particularly those on the upper surface of the packed bed, could jump up and have extra time and space to find a more fitting position to settle. For this reason, for a given mixture of particles, a higher rebounding probability tended to result in a denser packing structure. Another enforced constraint was that particles were not allowed to overlap. Because particles resided and moved on a lattice grid, collision and overlap detection was a simple matter of determining whether more than one object occupied the same lattice site(s) at any one time, rather than having to compute and test intersections between objects, which is usually the most computationally expensive part of vector-based particle simulations. Subsequently, trial moves that resulted in overlap were rejected. Despite its simplicity, the DigiPac algorithm has been shown to be able to satisfactorily predict poured bulk packing density in a variety of case studies involving both relatively large objects[12,13] and fine powders.[14]

Whereas the original version of DigiPac used random walks, in the new versions, particle movements are either wholly determined by laws of physics (in the case of DigiDEM) or partially guided by collisions (DigiCGP). Particles are still represented digitally, so that the ease and speed of collision/overlap detection and other computational advantages offered by the digital approach can be retained. Table 1 compares and contrasts the main features of, and highlights the differences between, the three versions. For the benchmark test case, the per-step CPU time of DigiDEM is less than 4 times that of the original DigiPac, but the total CPU time is many times more, because small time steps had to be used for numerical stability, requiring a much larger number of total steps to simulate the packing process. Significant speedup can be achieved if the simulations are run on a multi-CPU shared memory computer, as the software implementation is multithread enabled.

DigiDEM. The incorporation of DEM into the digital packing algorithm (DigiDEM) is to take into account the physical interactions between particles and between particles and container walls so that the algorithm can simulate more closely the final packed-bed structures. In this case, particle translations and rotations are no longer random but are governed by the contact and gravitational forces acting on the particle.

In contrast to the original DigiPac, a small amount of overlap between individual particles is permitted in DigiDEM to simulate deformations when particles come into contact with each other. Contact forces between particles are calculated based on these deformations (overlaps) at the voxel level. The voxel-level approach also accounts for rolling, friction, and other interparticle forces as normally considered in conventional DEM models. The main advantages of this approach compared to conventional DEM are greater simplicity and increased speed. These advantages are brought about by the fact that the faces of voxels are equally spaced and remain normal or parallel to the principal axes of the lattice-grid-mapped coordination system, even though the particles might be rotating. Also, complexity of the particle shape does not complicate software implementation of the algorithm. By measuring the number of contacts between two colliding/overlapping particles and their voxel-level contact forces, the force and torque acting on these particles can be calculated. The total force and torque acting on a particular particle are the sums of the interactions between the particle and all other particles or the container walls that

Table 1. Comparison of Different Versions of DigiPac

	DigiPac (original)	DigiCGP	DigiDEM
force	none, but effects of gravity and vertical vibration are incorporated by means of a so-called rebounding probability	each pair of colliding voxels given a unit nominal "force" along the line joining the collision point and the center of gravity of the particle	calculated from overlapping voxels, using the spring−dashpot contact force model
translation	random, one grid cell at a time	net collision force normalized against the largest component; each force component is between 0 and 1 and is used as a probability to move the particle one grid cell in that direction.	determined by force, velocity, and time step
rotation	random in both direction and angle, but the maximum angle of rotation is predefined.	"torque" calculated from nominal "forces", now normal to the colliding faces, and used as the axis of rotation	determined by torque, angular velocity, and time step
nature	stochastic	semistochastic	deterministic
inertia and momentum	no	no	yes
direct link with real time	no	no	yes
correlation with other physical properties	qualitative	semiquantitative	quantitative
benchmark test	single Xeon 2.66 GHz CPU, 886 short cylinders (27 × 27 × 18), 220 × 220 × 500 cylindrical container		
memory usage	41 MB	49 MB	1205 MB
steps required to form the packed bed	5600	3600	50000
CPU time per step after all particles are introduced	0.53 s	1.03 s	2 s
total wall-clock time	0.8 h	1 h	30 h

come into contact with the particle at a particular time step. Particle translational or rotational movement models are then established.

DigiDEM uses the spring−dashpot model for contact-force calculations between overlapping voxels.[15] The normal or tangential force due to an individual voxel−voxel contact is calculated as

$$F_{n,t} = (-k_{n,t}\delta_{n,t} - \eta_{n,t}v_{n,t})\vec{n}_{n,t}$$

where $k_{n,t}$, $\delta_{n,t}$, $\eta_{n,t}$, and $v_{n,t}$ are the stiffness, overlap, dumping coefficient, and relative velocity component, respectively, in the normal (denoted by subscript n) and tangential (denoted by subscript t) directions. In principle, more sophisticated contact force models can be used if available and desired.[16,17] In the simulations reported, the coefficients for the contact force model were determined through user experience, considering numerical stability, time-step interval (8×10^{-5} s), and maximum number of overlaps allowed. They were not determined from first principles based on material properties, because all particles were identical and we were concerned mainly with final packing structure, not the dynamics of the packing process itself. Additionally, as this version of DigiDEM implements only the simple spring−dashpot model, there are no choices for selecting different material properties.

DigiCGP. Rigorous treatment of the forces acting on each particle, such as in DigiDEM, comes at a high computational cost (Table 1). To identify trends, a quicker, albeit less accurate, solution is more desirable. DigiCGP is designed for this purpose. It is an intermediate solution, between the completely probabilistic and wholly deterministic extremes of the original DigiPac and DigiDEM, respectively. In DigiCGP, collision points are identified in the lattice grid, and each pair of colliding voxels is assigned a nominal impact force of 1. To calculate the torque, the direction of the nominal impact force is assumed to be normal to the contact face of the colliding pair of voxels. The net torque vector is later used as the axis of rotation for the particle in the next step. The angle of rotation is still random, but it is capped to give a maximum swept distance of no more than a few pixels during rotation. To calculate the net force, the direction of an impact force is taken to be along the line joining the collision point and the center of gravity of each particle. The reason for this can be illustrated by the case in which a particle, for example, a sphere, is dropped on a slope. Because of digitization, both the sphere surface and the slope are, at the voxel level, staircases. If the nominal impact forces were assumed to be normal to the local contact faces, the sphere would simply bounce vertically on the staircase rather than sliding down the slope, unless there happened to be contacts resulting in horizontal forces. Thus, for the determination of force and collision directions, a change in the direction of the impact force is a simple and effective short-cut, where the tangential force component is omitted. The net force is then normalized such that each orthogonal force component has a value between 0 and 1, which is later used as the probability for the particle to move, again one grid space at a time as in the original DigiPac, along each principal axis in the lattice grid.

Also as in the original version of DigiPac, the user-defined parameter of a rebounding probability is utilized. Therefore, all DigiCGP does is make use of collisions to decide the direction in which objects should attempt to move after a collision, meaning that objects have a tendency to move/rotate apart rather than follow a random motion. It should be noted that this treatment does not include voxel-level friction. However, particle-level friction is partially incorporated through the roughness of the digital surfaces. The model also neglects inertia effects, as particle velocity is neither calculated nor stored. All of these omissions are for the sake of speed. Table 1 shows that the simulation time of DigiCGP is comparable to that of the original DigiPac. For dense systems involving large and identical objects, such as the packed columns under investigation herein, the simplification is justifiable and acceptable, as demonstrated later.

3. Experiments

For experimental data reported in this work, two CT scanners were used. One (ULG 420kV scanner) is installed at Liège University and was used to scan a large (290-mm-diameter) packed bed of Pall rings; the other (Phoenix Nanatom) at Leeds University was used for smaller (≤50-mm-diameter) beds. The Liège scanner is a self-constructed X-ray tomography system[18] that is equipped with a linear detector of 1280 photodiodes. It can scan objects with a maximum diameter of 450 mm at a spatial resolution of 0.36 mm per pixel over a height of 3800

Table 2. Geometries of Pellets and Containers Used

name (code)	description	dimensions (mm)	digital version used in simulations ($W \times D \times H$ in pixels)
container 1 (LC)	plexiglas tube with a flat bottom of a rubber plug	44.5 (i.d.)	445 × 445 × 1200 CGP) 223 × 223 × 600 (DEM)
container 2 (SC)	Plastic tube (50 mL) with a slightly tapered trunk and a cone shaped bottom	28 (i.d., top) 100 (*H*, trunk) 24 (i.d., bottom) 15 (*H*, bottom)	300 × 300 × 1150 (CGP) 150 × 150 × 575 (DEM)
container 3	plexiglas column	290 (i.d.)	580 × 580 × 1200 (CGP) 290 × 290 × 500 (DEM)
alumina 38-OAT (A38)	short cylinders with flat ends	3.42 (*D*) 3.46 (*H*)	34 × 34 × 35 (CGP) 17 × 17 × 18 (DEM)
alumina 4 mm (A4)	short cylinders with indented doomed ends	4.99 (*D*) 4.20 (*H*)	50 × 50 × 42 (CGP) 25 × 25 × 21 (DEM)
Hama beads (HB)	plastic tubes	4.6 (o.d.) 2.5 (i.d.) 5 (*H*)	46 × 46 × 50 (CGP) 23 × 23 × 25 (DEM)
Pall rings (PR)	1-in. off-the-shelf plastic Pall ring pellets	25 (o.d.) 1 (wall thickness) 25 (*H*)	50 × 50 × 50 (CGP) 25 × 25 × 25 (DEM)

mm. The Nanotom is a 160-kV nanofocus CT scanner, equipped with a 5-megapixel (2304 × 2304 pixels) CCD detector and is capable of achieving a maximum pixel resolution better than 0.5 μm. The largest sample size the scanner can accommodate is approximately 60 mm across. As a generalized overview, the advantages of XMT are that it is a nondestructive, noninvasive method that is relatively fast (e.g., 2-h scanning time plus $^1/_2$-h reconstruction) and can give good levels of structural detail. On the negative side, the equipment is prohibitively expensive, and the edges of the structures tend to be blurred. Scanned images can also result in nonuniform shades (e.g., due to beam hardening), and the saved structures are subject to threshold errors.

Important geometrical characteristics of the pellets and containers used are listed in Table 2. With the exception of the Pall rings, in each case, the bed was scanned twice: once before tapping and once after tapping. The general procedure was as follows: The pellets were poured into the container, a handful at a time, with no tapping, vibration, or shaking until the height of the bed reached the top of the container. The bed was then scanned using the Phoenix Nanotom. After the poured bed had been scanned, the column was removed from the scanner and gently tapped on the side with a small L-shaped metal handle, reciprocated up and down several times, and then moved anticlockwise to a new angle, after which the same process was repeated until the column had been rotated one complete turn. Following this, the bed was pounded several times on the floor, with one hand holding around the base of the column and the other capping the top of the open container. Then, the bed was again tapped using the same handle, repeating the initial method of tapping. After the new height of the packing had been noted, the bed was rescanned, this time for the tapped density measurement.

The scan resolution was 0.024 mm, but reconstruction was done at one-quarter scale because of memory constraints of the computer. Thus, reconstructed images had a pixel resolution of 0.096 mm. Because of experimental limitations (namely, the height of the real packed columns), even at this lower resolution, the bed could not be fully accommodated by the view area. Therefore, XMT-scanned structures were applied to axial density profiles only in the central region of the packing, ignoring the region near the base wall. The reason for this is that, because the bulk structure is of the most practical interest for packed columns (which, in real applications, can be 10 m high but only several inches wide), from which mean bulk density measurements were to be calculated, it was considered vital to achieve a span that was expansive enough to provide a representative sample for reliable analysis. Wall effects in the context of DigiPac-generated packing structures have been extensively discussed elsewhere.[12,13]

There is only one CT data set for the Pall rings, because of the high cost of the experiment. This single scan corresponds to the tapped density. The packing and scanning were carried out by pouring the Pall rings into a 290 mm (i.d.) Plexiglas column to obtain a 1-m-high packing. The bed was then mixed with a rod until large visible heterogeneities disappeared, and the column was then tapped. A total of 269 successive scans, separated by 0.5 mm in height, were then performed around the central section of the packed column. Each reconstructed cross section was an 879 × 879 pixel square, with a pixel resolution of 0.36 mm.

In addition to the bulk density and local density distribution, other structural metrics, such as two-point correlation functions, have been proposed for porous media.[19] These were not used for comparison between scanned and simulated structures in this study, as these statistics lump together contributions from both intra- and interpellet pore structures. At least for Pall rings, the complex pellet geometry means that the contribution from the intrapellet structure was likely to be overwhelming. Thus, comparing such statistics would not have served the purpose of model validation for packing (i.e., interpellet) structures. Because all of the pellets used in this study were essentially cylindrical and most can be considered to be axially symmetric, it was decided that the axial orientation distribution of the pellets would be a more appropriate metric than correlation functions for our purposes.

4. Results and Discussion

A selection of scanned and simulated packed beds of generic pellet shapes is reported here. They involve four types of pellets in three different containers, as indicated in Table 2. With the exception of Pall rings, multiple beds were scanned before tapping (denoted poured) and after tapping (denoted tapped), and at least as many simulations were performed using the two new versions of DigiPac (CGP and DEM). For both models, the pouring of particles was simulated by dropping a small number of pellets each time from random points within a circular area above the container (which also had a circular cross section). This approach was in line with how pellets were introduced in the packing experiments. Another point to note is that preliminary tests showed that shaking, by lifting the bed

Table 3. Summary of Experiments and Simulations

case	CT scans	CGP simulations	DEM simulations	mean bulk density (stdev)[a]		
				CT scans	CGP simulations	DEM simulations
A38 in LC poured	4	5	5	0.591 (0.006)	0.600 (0.006)	0.577 (0.014)
A38 in LC tapped	4	−	5	0.646 (0.008)	−	0.613 (0.014)
A4 in LC poured	5	5	9	0.568 (0.009)	0.568 (0.012)	0.540 (0.021)
A4 in LC tapped	5	−	9	0.607 (0.011)	−	0.599 (0.020)
HB in LC poured	3	5	6	0.386 (0.008)	0.399 (0.010)	0.384 (0.015)
HB in LC tapped	3	−	6	0.434 (0.009)	−	0.418 (0.014)
HB in SC poured	3	6	7	0.390 (0.019)	0.378 (0.017)	0.356 (0.025)
HB in SC tapped	3	−	7	0.445 (0.010)	−	0.386 (0.027)
PR poured	0	1	4	−	0.109 (0.004)	0.115 (0.004)
PR tapped	1	−	4	0.090 (0.005)	−	0.123 (0.004)

[a] Standard deviations in parentheses.

en masse and letting it resettle, as used to simulate tapping in the DEM model, made little difference to the results of CGP simulations, which ignore inertia and the velocities of particles. For this reason, tapping was not performed in the CGP simulations. The results are summarized in Table 3, with selected beds analyzed in more detail later in this section. It is interesting to note that, whereas bulk packing densities from CGP simulations are closer to the poured bulk densities in the measured experimental beds (Table 3), orientation distributions generally sit between the poured and the tapped results, leaning toward the tapped, as exemplified in Figures 3c, 4c, and 5c, below.

With regard to Table 3, some general comments are in order. The mean bulk densities were obtained by averaging the axial density profiles in the middle section of the packed columns (i.e., in terms of vertical height). The trend in the mean bulk density as displayed by the CT data, in terms of pellet/container geometry changes, is followed by the results from both the CGP and DEM simulations. The density increase due to tapping as observed in the CT data sets, which ranges between 7% and 14%, is also reflected in the DEM results, which show a similar increase ranging between 7% and 11%. Standard deviations (stdev in Table 3) were also calculated from the axial density profiles. They are a measure of density variations within the packed beds, not between the beds. In other words, these stdev values are an indicator of how uniform the bed structures are in the middle (i.e., bulk) section in each case. The level of density fluctuation within the CT-scanned beds is approximately the same as the CGP-simulated values and about one-half the DEM simulated values. The increased fluctuation in the DEM simulations is attributed to the fact that DEM simulations were performed at one-half the scale for the sake of speed. Lower resolution usually results in higher digitization errors, which can be further aggravated during the simulations by particle rotation.

Figure 1 contains some examples of the packed beds used in this study. The visual similarities are evident, bearing in mind that they are random packing structures and one-to-one correspondence cannot be expected.

Packing of Alumina 38-OAT Pellets in LC. These are alumina cylinders with a mean diameter of 3.42 mm and a height of 3.46 mm. Based on the XMT data, the mean bulk density, excluding end effects, was estimated to be 0.591. DigiCGP estimates bulk density at 0.600, 1.5% higher than the CT estimate. For the DigiDEM simulations, which were carried out at one-half the scale of the CGP runs, bulk density was calculated as 0.577, 2.37% lower than the mean determined for the experimental beds. Figure 2 compares the measured and simulated results for A38 pellets poured in the LC container. Figure 2a shows poured axial density profiles. The distance is scaled by the pellets' mean diameter. As the CT data show only the middle, bulk section, the profile drops at both ends. The CGP, DEM, and CT profiles cross one another at numerous points, and their means differ by less than 3%. The radial density distributions of the poured beds (Figure 2b) show that the simulations qualitatively predict the mean profile of the CT-scanned beds. Close to the container wall, the radial density distribution varies in an oscillatory manner, with the amplitude of density oscillations becoming progressively damped with increasing distance from the container wall. The maximum radial density value for both packing models and the CT bed occurs at approximately 1.5 particle diameters, and the minimum radial density for all three methods, excluding the value at the wall, occurs at approximately 2.5 particle diameters into the packing matrix. Figure 2c shows vertical orientation distributions for beds containing poured A38 pellets that were calculated automatically for CGP, DEM, and CT structures using the modified Markov chain Monte Carlo (MCMC) procedure (see the Appendix). The CT beds exhibit a higher proportion of pellets oriented toward the midrange angle groups, in the form of an inverted V shape. The CGP results qualitatively reproduce the orientation angles of the experimental results. However, too few pellets lie in the low-range angle groups (0−40°), whereas an excessive number of particles are observed in the midrange groups (40−60°). Overall, the CGP prediction of orientation distribution is poor. For DEM, a significant improvement is seen in the prediction of orientation over that of the CGP model, although discrepancies still exist in the minimum and maximum angle groups. In DEM mode, the predictions quantitatively agree with the X-ray CT results within acceptable error margins.

Following tapping of the experimental and DEM beds, larger discrepancies between the measured and predicted results were evident, as can be observed in Figure 3. Figure 3a displays the axial packing density of tapped A38 pellets. These profiles show that the CGP (poured) and DEM models underestimate the packing density of the averaged CT beds. The increased sinuous fluctuations present for the tapped radial density distributions, as shown in Figure 3b, arose as a result of tapping. Compared to the poured beds, the fluctuations after tapping extend much farther into the center of the beds, and the first peak is higher. These trends are qualitatively followed by the simulations, but quantitatively, the differences are very noticeable. Vertical orientation distributions for beds of tapped A38 pellets are displayed in Figure 3c. The poured CGP results again fail to closely match the orientation angles of the tapped CT-scanned results. Most noticeable is that a disproportionate number of pellets are in the 40−50° angle group. Additionally, too few pellets are in higher groups (60−80°) compared to the mean CT data. With CGP, a general trend observed from comparisons with experimental data is that the poured pellet orientation distributions tend to be between the poured and tapped real beds, with orientations closer to those of the tapped beds. With DEM, a noticeable improvement is seen in the prediction of the

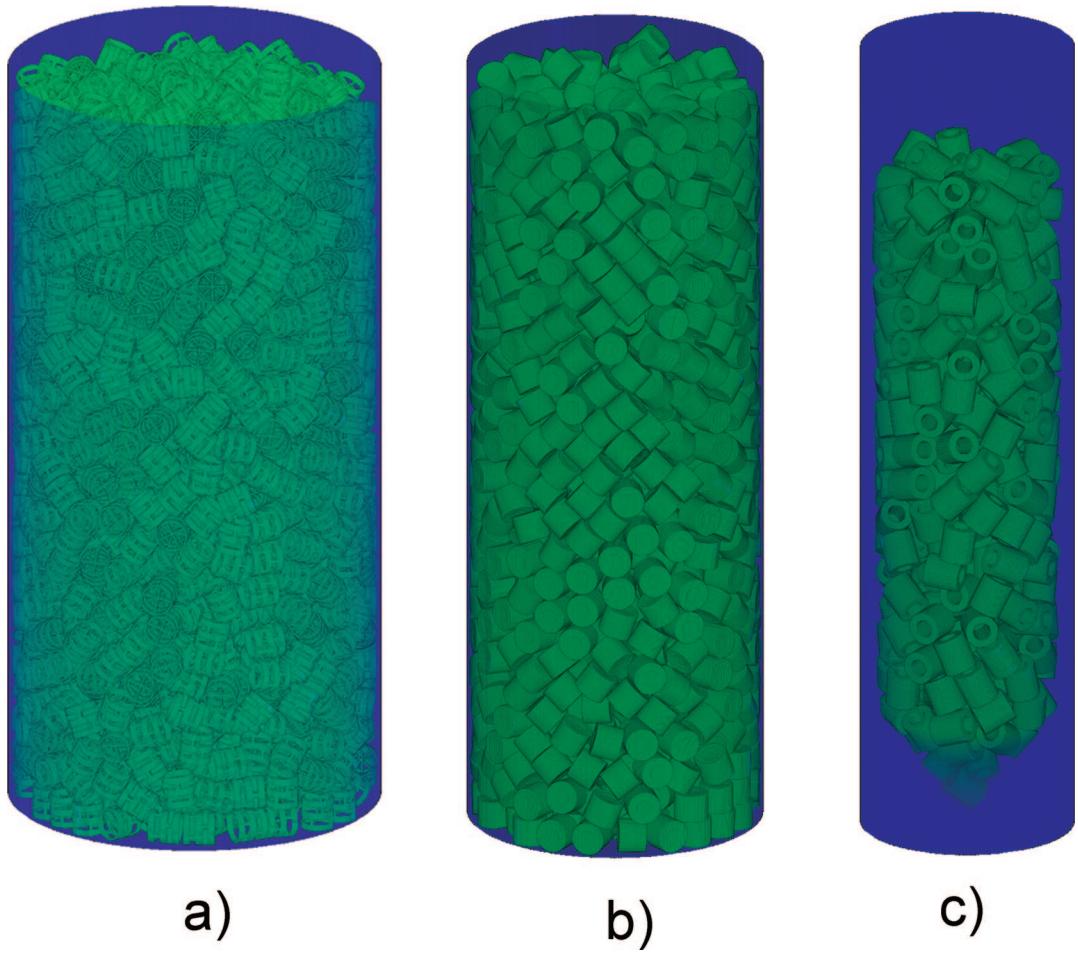

Figure 1. Visual examples of the beds used in this study, as obtained from the simulations: (a) Pall ring packing, (b) packing of 4-mm alumina pellets, (c) Hama beads packing.

orientation distribution. In DEM mode, the tapping results in a denser packing structure and, more importantly, changes in orientation distribution in the same manner as revealed by X-ray CT scans.

Packing of Hama Beads in SC. Hama beads are hollow cylinders with a mean diameter of 4.6 mm, a length of 5.0 mm, and a central hole that is 2.5 mm in diameter. The container used was a 50 mL tube, with a tapered cylindrical trunk and cone-shaped bottom end (Figure 1c and Table 2). The mean bulk density after pouring as estimated by the CT-scanned structures is 0.390, increasing to 0.445 following tapping. Both models underpredict this value, with poured values of 0.378 and 0.356 for CGP and DEM, respectively. Following tapping, the DigiDEM model estimates a bulk density of 0.386. Figure 4 compares experimental and simulation data after tapping. For axial density (Figure 4a), both models underestimate the CT-scanned structure. The relatively poor agreement in mean bulk density between the measured and predicted beds is exacerbated by both statistical errors and the fact that the simulated tapping did not precisely match the tapping of the experimental beds. Statistical errors arise from three sources: First, repacking was undertaken only three times for CT-scanned structures (tapped) compared to seven times for DEM beds. Second, X-ray-scanned structures were made binary by applying a single threshold throughout the structure. The bulk density is sensitive to this threshold—a slightly different threshold can easily shift the bulk density up or down. Third, digitization errors exist in both X-ray-scanned and simulated beds as both are digitally specified. Such errors tend to be exacerbated for boundaries that are diagonal, i.e., not aligned with the axes of the lattice grid. Recognizing these inherent sources of errors, the goal was not to seek exact numerical match, but to compare the trends (in terms of pellet shape, pellet/column size ratio, and packing method versus bulk density and pellet orientations) and the extent of fluctuations in the density plots. In these two aspects, the simulations and experiments are comparable.

The radial density profiles (Figure 4b), although still oscillating as in the previous A38 case, display a more complex pattern, because of the presence of holes in the pellets. Being plastic, Hama beads are expected to be less affected by impact forces and momentum exchanges and, therefore, more amendable to the CGP model. For orientation distributions (Figure 4c), the agreement between the three methods is noticeably better than for the alumina A38 pellets. However, the CGP-simulated structures still contain a disproportionately large number of pellets in the 30−50° groups. For the DEM results, because of their low resolution, some fine details in the radial density profiles are lost, but the simulated orientation distribution compares very well with the measured results.

Packing of Pall Rings. These are 1-in. Pall rings with a mean diameter of 25 mm and a height of 25 mm, poured into a cylinder of 290-mm inner diameter, stirred to promote uniformity, and then tapped. The tapped bulk density of the single scanned bed was estimated to be 0.090, close to the manufacturer's value of 0.091. The predicted bulk densities, averaged in the central section to correspond with the XMT bed, were 0.109 (CGP) and 0.123 (DEM). Figure 5 compares the local voidage and orientation results. The axial density distributions

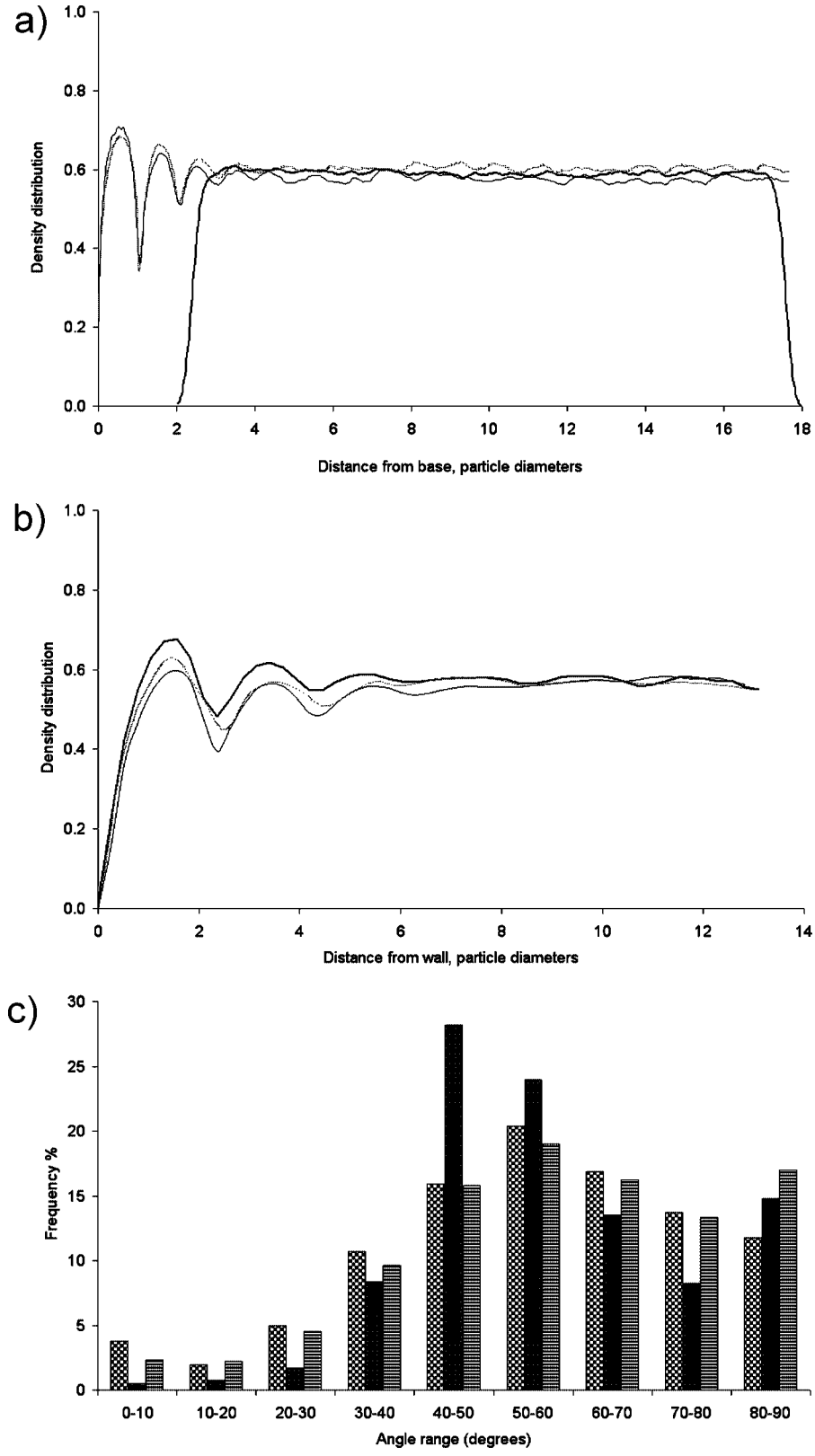

Figure 2. Comparisons for A38 in LC, poured: (a) axial density profiles, (b) radial density profiles, (c) vertical orientation distributions. (CT = thick solid line/chessboard pattern, DEM = thin solid line/barcode pattern, CGP = dotted line/shaded pattern.)

of the simulated Pall ring beds (Figure 5a) again underestimate the CT-scanned structure, although qualitative agreement does exist. The radial density for beds packed with Pall rings (Figure 5b) displays qualitative agreement between the measured and predicted beds, particularly near the wall ($\leq$2.0 particle diameters), which suggests that the presence of the wall structure combined with the deterministic nature of DigiDEM influences how the particles pack. Farther into the bed, a reasonable qualitative agreement still exists, but comparative results suggest a greater degree of randomness to the packing.

Note that the vertical scale used for the density profiles is much smaller than in Figures 2−4, in order to show the details,

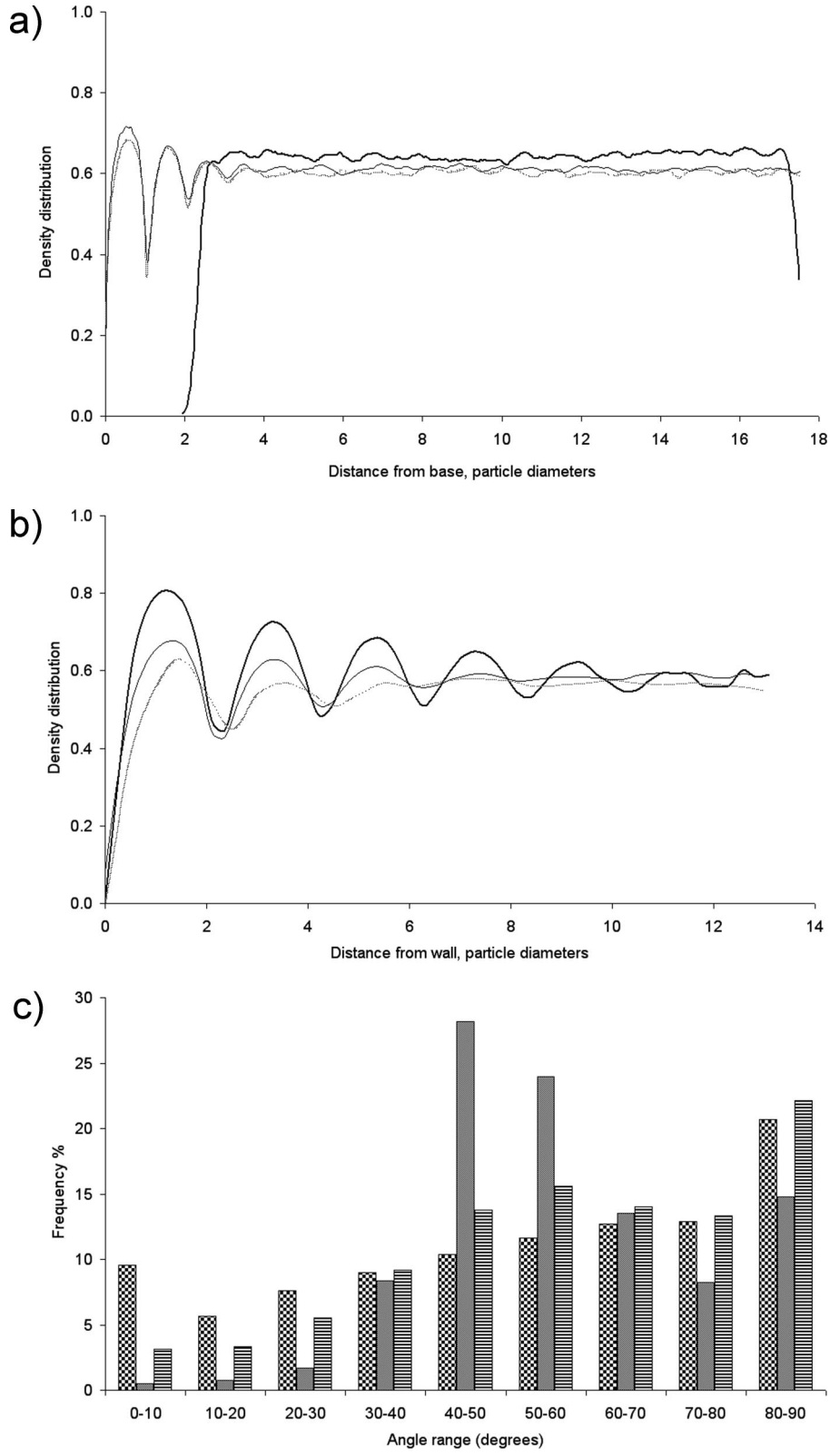

Figure 3. Comparisons for A38 in LC, tapped: (a) axial density profiles, (b) radial density profiles, (c) vertical orientation distributions. (CT = thick solid line/chessboard pattern, DEM = thin solid line/barcode pattern, CGP = dotted line/shaded pattern.)

but this also visually amplifies the discrepancies, believed to be mainly due to digitization errors. In the original CT scan data set, the horizontal pixel resolution was about 0.36 mm, and the vertical resolution was about 0.5 mm. The data set was rescaled such that each voxel had the same pixel resolution in all three principal axes (0.5 mm/pixel). At this resolution, the thickness of the pellet wall should be two pixels. However, after rescaling and thresholding, the walls in the CT bed appear thinner and less uniform than in the CGP beds, which have the same pixel resolution. In the DEM simulations, the wall is one pixel thick, but when magnified to the same scale, again the pellet walls appear thicker than in the CT bed. Another

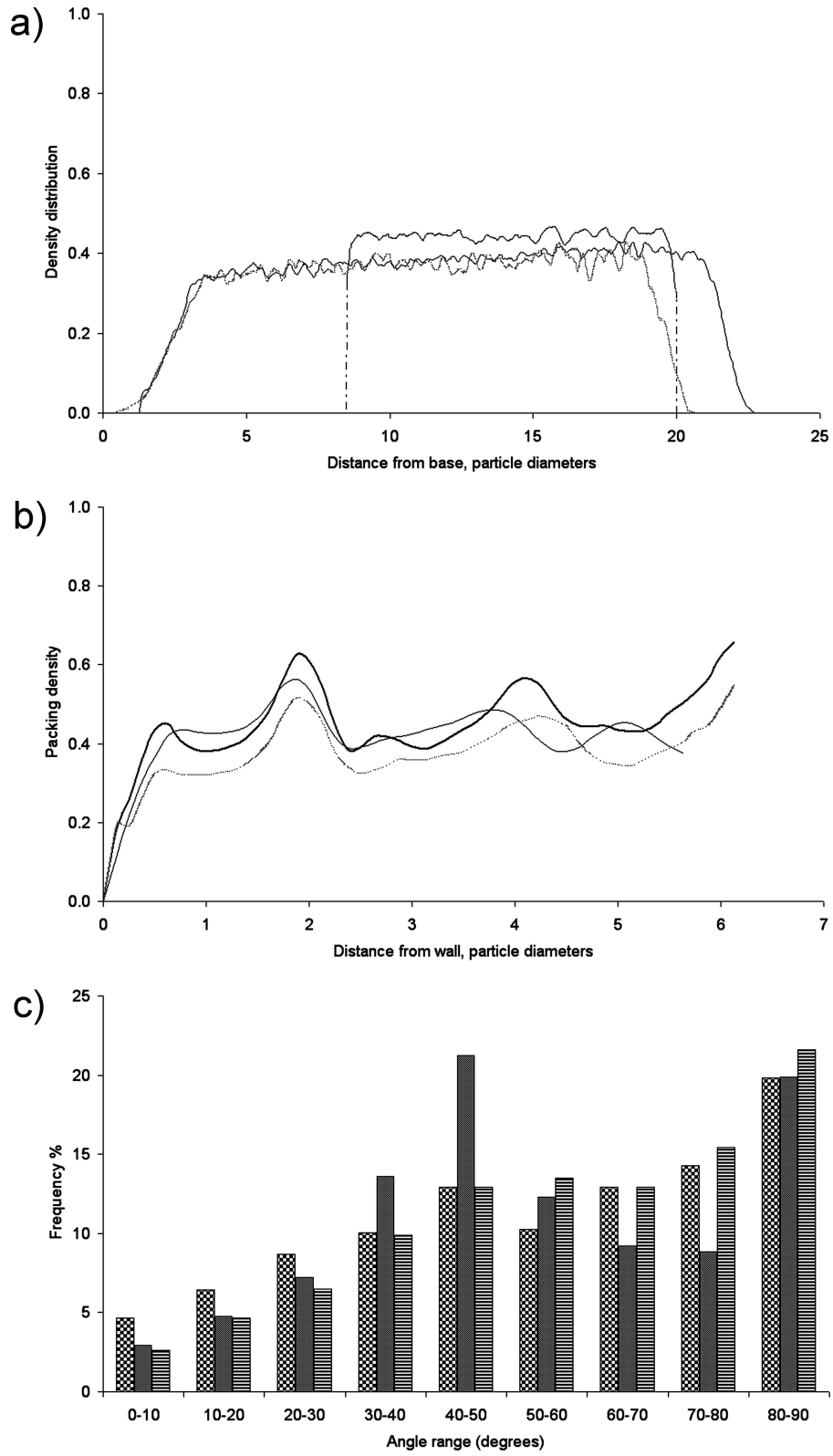

Figure 4. Comparisons for Hama beads in SC, tapped: (a) axial density profiles, (b) radial density profiles, (c) vertical orientation distributions. (CT = thick solid line/chessboard pattern, DEM = thin solid line/barcode pattern, CGP = dotted line/shaded pattern.)

difference is that, in the simulations, the column has a diameter of 580 (CGP) or 290 (DEM) pixels, but the processed CT bed is 576 pixels wide (i.e., a deficiency of four pixels compared to CGP). Finally, there are statistical errors. There is only one CT data set because of the high cost of the experiment compared to four for the DigiDEM simulation model. Despite all of these minor but fundamental differences between the measured and predicted beds, given the complexity of the pellet geometry, the agreement between experiment and simulation is considered to be reasonably good.

Discussion. For all of the packed columns considered in this work, several factors can contribute to the discrepancies seen for both local density and orientation distribution between measured and predicted results. First, both CT-scanned and

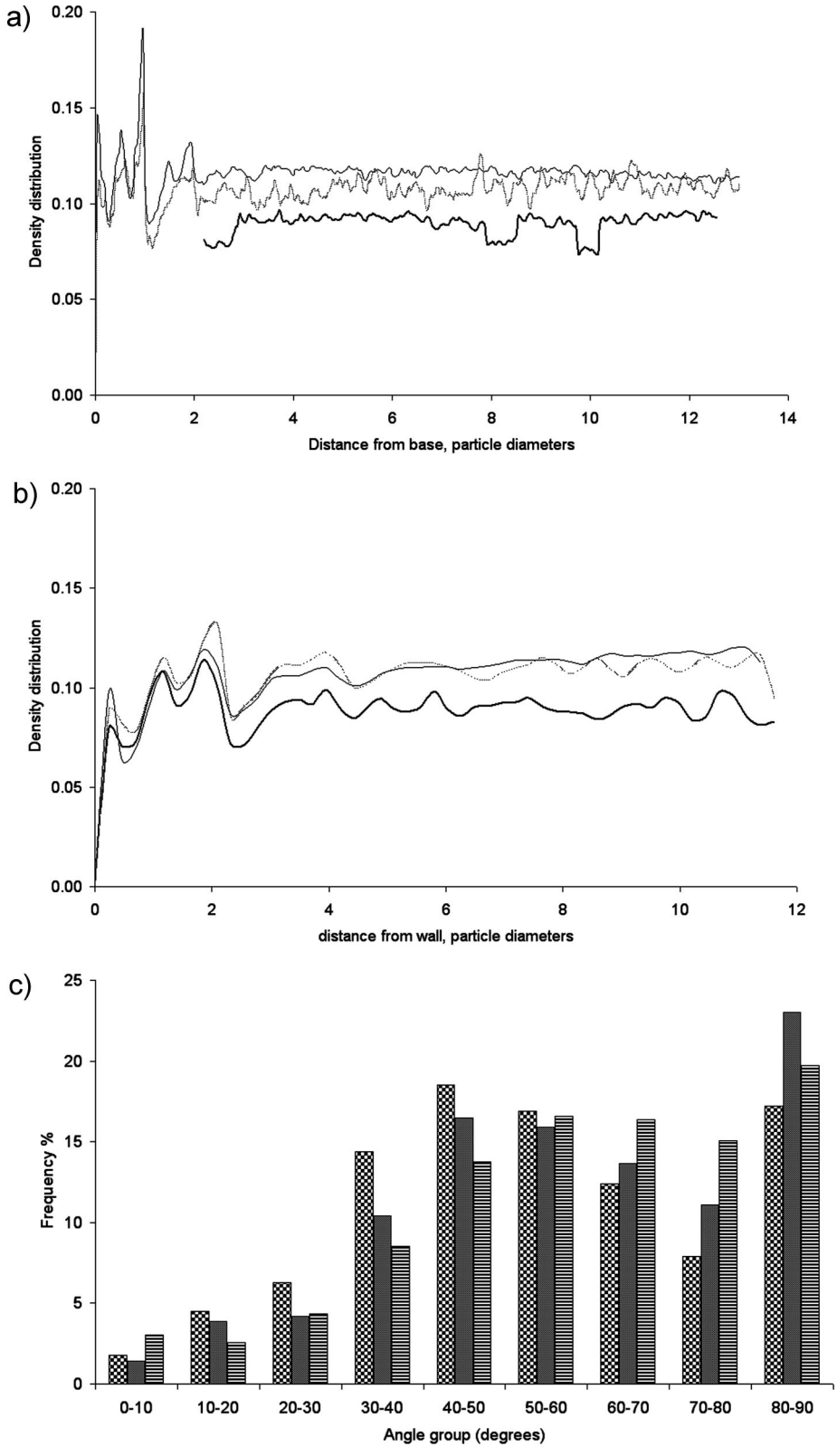

Figure 5. Comparisons for rings, tapped: (a) axial density profiles, (b) radial density profiles, (c) vertical orientation distributions. (CT = thick solid line/chessboard pattern, DEM = thin solid line/barcode pattern, CGP = dotted line/shaded pattern.)

DigiPac-simulated structures contain digitization errors. For the sake of speed, simulations were performed at much a lower resolution than for the CT scans (0.096 mm/voxel for CT-scanned beds; see Table 2 for comparisons with simulated beds). Second, and still on the subject of digital errors, there is another difference between scanned and simulated beds. In DigiPac, pellets are input in digitized form and rotated digitally. Digital rotation introduces two more errors: one easily quantifiable, the other not so. Errors of the first kind are small and, at reasonably fine resolutions, usually less than 1% (by volume). A volume-conservation procedure is employed to ensure that they do not accumulate, but it does not guarantee that pixel-level morphology is preserved at the same time. In DigiDEM, because contact forces are calculated at the pixel level, an extra pixel here and

a missing pixel there on a particle surface can make a difference in the calculated net force/torque. Such errors are inherent in the digital approach, no matter how high the resolution is, and it is difficult to quantify the effects of these errors in a random packing. Further investigation and algorithmatic improvement are needed, as such errors are not present in CT-scanned structures. Third, in the case of tapping, the simulations did not exactly match the physical act of tapping. Again, for the sake of speed, in DEM, tapping was simulated instead by periodically giving the bed an upward momentum (i.e., velocity), enough to lift it off the ground, and then allowing the bed to resettle. In CGP, where velocity is not considered explicitly, initial trials in which the bed was repeatedly lifted en masse to a certain height and then allowed to resettle showed little change from the poured structures. The difference between the DEM and CGP treatments is that, in DEM, momentum is allowed to play a role, whereas in CGP, it is not. The role of momentum in the packing of relatively large particles in a confined space turns out to be a significant one, as evident from the above comparisons of results: the DEM results are generally in a better agreement with the CT results. Fourthly, real pellets do vary in size. As an example, the A38 pellets are the product of extrusion, as is reflected in their heights. When this is the case, the variation can then be assessed by weighing the pellets. A batch of 100 A38 pellets weighed about 7.60 g, but when 10 of the pellets were weighed individually, the average was 0.078 g, ranging between 0.071 and 0.084 g, with a sample standard deviation of 0.0043. Some broken pieces were also present in the real beds. Such variations in pellet size are expected to have an effect on the microstructure of the beds, but this effect was not considered in the simulations, which used identical pellets. Finally, although more than one data set was used in most cases, the number was not high enough to rule out statistical errors. This applies to both CT-scanned and DigiPac-simulated results. For example, in radial density distributions of the four CT-scanned A38 beds (tapped), the value of the first maxima ranges between 0.78 and 0.83, and farther into the core, the difference becomes even larger, 0.50−0.67. Corresponding values from the five CGP simulations are 0.68−0.75 at the first peak and 0.54−0.70 at the center. From DEM, the values are 0.71−0.76 and 0.57−0.66, respectively. In conclusion, when all of these sources and ranges of errors from both experiments and simulations are taken into account, the numerical discrepancies are expected but are considered to be within a reasonably acceptable range.

5. Conclusions

Packed beds of cylindrical pellets of different size and complexity were tomographically scanned and compared with simulations obtained using two new versions of the DigiPac model. The comparison was performed in terms of bulk packing density, axial and radial density profiles, and pellet orientations. Whereas the original stochastic DigiPac model is able to qualitatively follow the trend in bulk packing density, the new versions, which incorporate the effects of particle interaction forces at different levels of rigor, have been demonstrated to provide more accurate predictions of the packing structures at the particle level. Given the complexity of the problem and the errors in both the experimental and simulation data sets, it can be said that the agreement between experiments and simulation is good and within the practically acceptable error range as determined by our industrial partner. Thus, DigiCGP and DigiDEM can be used as design or optimization aides, insofar as packing structure is concerned, for packed columns. DigiCGP is much faster but less accurate, suitable for initial screening, whereas DigiDEM is quantitatively more accurate but much slower and thus suitable for fine-tuning. Future research programs will focus on the following aspects: model validation for a wider range of pellet shapes, development of numerical techniques that can make direct use of these digitally specified microstructures for prediction of other properties of interest, improvement of simulation speed, and better ways to quantify and deal with digital errors.

Acknowledgment

Financial support from the U.K. Engineering and Physical Sciences Research Council, EPSRC, Grant EP/D503078/01, is gratefully acknowledged.

Appendix

Details on the procedure for data extraction and postprocessing of simulated and XMT-scanned beds are provided in the following sections.

Calculation of Local Packing Density

For digitally specified packing structures, the density and density distribution were calculated by counting the solid voxels and dividing the count by the total number of grid cells within the corresponding packing space. This procedure was applied to both simulated and CT-scanned packing structures. We first consider the packing density in the axial direction, i.e., from the base of the bed upward toward the surface. The packing density of each bed slice, one voxel in height, was calculated, with the process repeated for every slice of the packed bed. The values were then plotted against axial distance from the base of the container in units of particle diameters. Bulk packing density was calculated by averaging the axial packing density after end effects had been excluded. To calculate the radial packing density, the column was divided into equally spaced concentric rings, and again, voxel counting was used, this time for each ring over the total height of the bed, rather than for each slice. The values obtained were then plotted against radial distance in units of particle diameters from the retaining wall.

Calculation of Pellet Orientation Distribution: MCMC Procedure

We used the technique of Markov chain Monte Carlo (MCMC) here to help extract pellet information. The position, p, of a pellet P in a packed structure can be described by a set of seven parameters $p = \{x, y, z, a_x, a_y, a_z, a\}$, where $\{x, y, z\}$ is the location and $\{a_x, a_y, a_z, a\}$ represents the rotation axis and rotation angle relative to the local coordinate system of the pellet. In the digital approach, the digital image of pellet P, denoted by s, can be described by a set of gray-scale voxels $s = \{s_1, s_2, ..., s_n\}$, where $n = n_1 \times n_2 \times n_3$ and n_1, n_2, and n_3 are the dimensions of the bounding box of P. For a proposed pellet Q to fit P, the digitization of Q forms another set of gray-scale pixel image $t = \{t_1, t_2, ..., t_n\}$. If we assume Gaussian noise for image s, the likelihood of fitting Q to P is then

$$L(s;\{x,y,z,a_x,a_y,a_z,a\}) = \left(\frac{1}{\sqrt{2\pi}\sigma}\right)^2 \prod_{i=1}^{n} \exp\left(-\frac{d_i^2}{2\sigma^2}\right)$$

where $d_i = |s_i - t_i|$ and σ^2 is the noise variance.

If we assume that there is no preferential factor affecting the position of P, we can use uniform priors for any of the

parameters of p, i.e., uniform distributions for locations, rotation axis, and rotation angle. The combination of the priors and the likelihood above gives the posterior density $\pi(\{x, y, z, a_x, a_y, a_z, a\}|s)$. One way to calculate the posterior means (the most likely values of the parameters) is by the technique of MCMC simulation. The simulation produces a Markov chain whose equilibrium distribution is the posterior (target) density $\pi(\cdot)$. If Q is randomly placed in the packed column and if the generated Markov chain is long enough, the chain will eventually settle at its equilibrium state. The most likely values of $p = \{x, y, z, a_x, a_y, a_z, a\}$ can then be estimated from $\pi(\cdot)$. Detailed descriptions of MCMC and the sampling strategy are beyond the scope of the work. We refer interested readers to additional material for a practical introduction to the technique.[20]

Postprocessing of XMT-Scanned Beds

The scanning was carried out in the Phoenix Nanotom machine with the following settings: 150 kV; 100 μA; 1440 projections; 500-mS exposure time; and three-frame averaging, skipping one frame. Detector calibration was performed only once, and the offset and gain map were saved and used for all subsequent scans. However, for each scan, a separate alignment correction was done. The scan resolution was 0.024 mm, but reconstruction was done at one-quarter scale (0.096 mm/pixel) because of memory constraints of the computer. The reconstructed volumes were cleaned by a single global thresholding. The threshold was selected such that the diameter of perfect circles in the reconstructed slices conformed to the measured average pellet diameter (based on measurement of 30 or more randomly selected pellets from each sample). After being cleaned, the scanned bed structures were analyzed in the same way as the simulated structures, for bulk density, local density distribution, and pellet orientation distribution.

The Pall-ring orientation distribution was calculated manually, by first eroding the 3D binary volume to isolate individual pellets. Because the rings are straight cylinders, their axes can be determined using two center-axis points per pellet. Whole circles or ellipses were selected from different Z-axis slices, two center-axis coordinates were recorded for each individual pellet, and the angles were calculated in relation to the column axis. The remaining majority of the pellet information for the other beds was extracted using the MCMC procedure summarized previously. Only the Pall ring bed was done by hand as the MCMC program was not completed at that time.

Literature Cited

(1) Strigle, R. F., Jr. *Packed Tower Design and Applications: Random and Structured Packings*, 2nd ed.; Butterworth-Heinemann: Boston, MA, 1994.

(2) Ridgway, K.; Tarbuck, K. J. Voidage Fluctuations in Randomly-Packed Beds of Spheres Adjacent to a Containing Wall. *Chem. Eng. Sci.* **1968**, *23*, 1147.

(3) Roshani, S. Elucidation of Local and Global Structural Properties of packed-bed Configurations. Ph.D. Thesis, Department of Chemical Engineering, University of Leeds, Leeds, U.K., 1990.

(4) Vatani, A. Characterisation of Transport Processes in Packed Beds. Ph.D. Thesis, Department of Chemical Engineering, University of Leeds, Leeds, U.K., 1996.

(5) McGreavy, C.; Foumeny, E. A.; Javed, K. H. Characterisation of Transport Properties for Fixed Beds in Terms of Local Bed Structure and Flow Distribution. *Chem. Eng. Sci.* **1986**, *41*, 787.

(6) Jia, X.; Williams, R. A. A Packing Algorithm for Particles of Arbitrary Shapes. *Powder Technol.* **2001**, *120*, 175.

(7) Ramaioli, M.; Pournin, L.; Liebling, Th. M. Brazil Nut's Effect Beyond Spherical Grains: Elongation Matters! Presented at the Fifth World Congress on Particle Technology, Orlando, FL, Apr 23−27, 2006.

(8) Seidler, G. T.; Martinez, G.; Seeley, L. H.; Kim, K. H.; Behne, E. A.; Zaranek, S.; Chapman, B. D.; Heald, S. M. Granule-by-Granule Reconstruction of a Sandpile from X-ray Microtomography Data. *Phys. Rev. E* **2000**, *62*, 8175.

(9) Richard, P.; Philippe, P.; Barbe, F.; Bourlés, S.; Thibault, X.; Bideau, D. Analysis by X-ray Microtomography of a Granular Packing Undergoing Compaction. *Phys. Rev. E* **2003**, *68*, 020301.

(10) Aste, T.; Saadatfar, M.; Sakellariou, A.; Senden, T. J. Investigating the Geometrical Structure of Disordered Sphere Packings. *Physica A* **2004**, *339*, 16.

(11) Zhang, W.; Thompson, K. E.; Reed, A. H.; Beenken, L. Relationship between Packing Structure and Porosity in Fixed Beds of Equilateral Cylindrical Particles. *Chem. Eng. Sci.* **2006**, *61*, 8060.

(12) Caulkin, R.; Fairweather, M.; Jia, X.; Williams, R. A. A Numerical Investigation into the Simulated Packing of Multi-Tubular Catalytic Reactors. Presented at the 5th International Conference for Conveying and Handling of Particulate Solids, Sorrento, Italy, Aug 27−31, 2006.

(13) Caulkin, R.; Jia, X.; Fairweather, M.; Williams, R. A. An Investigation of Catalyst Packed Columns Using DigiPac. *Comput. Chem. Eng.* **2006**, *30*, 1178.

(14) Jia, X.; Gan, M.; Williams, R. A.; Rhodes, D. Validation of a Digital Packing Algorithm in Predicting Powder Packing Densities. *Powder Technol.* **2007**, *174*, 10–13.

(15) Xu, C.; Jia, X.; Williams, R. A.; Stitt, E. H.; Nijemeisland, M.; El-Bachir, S.; Sederman, A. J.; Gladden, L. F. Property Predictions for Packed Columns Using Random and Distinct Element Digital Packing Algorithms. Presented at the Fifth World Congress on Particle Technology, Orlando, FL, Apr 23−27, 2006.

(16) Cundall, P. A.; Strack, O. D. L. A Distinct Numerical Model for Granular Assemblies. *Geotechnique* **1979**, *29*, 47.

(17) Munjiza, A. *The Combined Finite−Discrete Element Method*; Wiley: New York, 2004.

(18) Toye, D.; Crine, M.; Marchot, P. Imaging of Liquid Distribution in Reactive Distillation Packings with a New High-Energy X-ray Tomograph. *Meas. Sci. Technol.* **2005**, *16*, 2213.

(19) Torquato, S. *Random Heterogeneous Materials: Microstructure and Macroscopic Properties*; Interdisciplinary Applied Mathematics Series; Springer-Verlag: New York, 2001; Vol. 16.

(20) Gilks, W. R.; Richardson, S.; Spiegelhalter, D. J. *Markov Chain Monte Carlo in Practice*; Chapman & Hall: Boca Raton, FL, 1996.

Received for review January 09, 2008
Revised manuscript received June 19, 2008
Accepted June 27, 2008

IE800033A